Scuola di Scienze Matematiche Fisiche e Naturali
Laurea triennale in Fisica e Astrofisica

Small pitch pixel detector for the CMS phase II upgrade

Intern:
Irene Zoi

Supervisor:
Gino Bolla,
Lorenzo Uplegger

Summer Program 2015

Contents

List of Figures

Introduction

During my intern period I worked for the CMS Pixel Phase II collaboration. The innermost part of the CMS detector is the tracking system made of silicon pixels and strips. It allows to reconstruct the trajectories of all charged particles that pass trough it. The tracker will be replaced, phase II upgrade, following the luminosity increase of the LHC. I studied a prototype for the pixel detector upgrade with a much smaller pitch with respect to the current one. In particular I analyzed the data collected during the test-beam that took place in June 2015 at Fermilab Test Beam Facility (FTBF). During my two months stay, I focused my attention analyzing the collected charge and measuring the detector spatial resolution.

This report is the summary of my experience at Fermilab.

Chapter 1

The CMS experiment at CERN

CMS (Compact Muon Solenoid) is one of the experiments at the Large Hadron Collider (LHC) located at the *Conseil Européen pour la Recherche Nucléaire* (CERN) in Geneva, Switzerland [1].

LHC is the largest and highest-energy particle accelerator in the world. It consists of two separate beam pipes to accelerate protons in opposite directions up to an energy of 7 TeV each.

There are four main experiments placed in the interaction point along the 27 km circumference ring in order to measure the decay products of the colliding particles.

CMS, one of the two multi purpose detectors, is built in a cylindrical structure as shown in figure **??**. It consists of several sub - detectors to precisely measure tracks and energies of the particles produced in the collisions: from inside out, the tracker to reconstruct the trajectories of all charged particles, the electromagnetic calorimeter to measure the energies of photons and electrons, the hadron calorimeter to measure the energies of hadrons, the coil of the solenoid to provide a 3.8 T magnetic field and the iron return yoke of the solenoid interlaced with muon chambers to measure the momenta of muons.

1.1 The tracking system

The tracking system must allow a precise measurement of charged particle trajectories and reconstruction of secondary vertices. To do so, good position and momentum resolution and a high reconstruction efficiency are required because of the high luminosity of 10^{34} $\mathrm{cm}^{-2}\mathrm{s}^{-1}$ and the short time of 25 ns between bunch crossings that lead to 40 million expected events per second, each resulting in about 1000 particles. In order to achieve the goals the detector must have a high granularity but a low occupancy per bunch crossing. Also, the readout of the detector must be fast and the entire system has to be radiation hard. Due to these requirements, the tracking system has a full silicon detector with decreasing granularity from inside out. To avoid a too high leakage current the whole tracker is cooled at a temperature of -10℃.

1.1.1 The silicon pixel detector

It is the innermost part of the tracking system. It is located around the beam pipe and therefore close to the interaction point.

It must have a very good spatial resolution. This is realized by a small size of the pixels ($100\mu\mathrm{m}\times150\mu\mathrm{m}$ for Phase I) and by the fact that the produced charge inside a sensor of the detector is shared between pixels.

The silicon pixel detector consists of three barrel layers placed radially around the beam pipe, at a distance of 4.4 cm, 7.3 cm, and 10.2 cm, and two disks at z= $\pm$34.5 cm and z= $\pm$46.5 cm as visible in figure 1.1. It has 66 million channels in total. The barrel part is built of 672 modules and 96 half-modules.

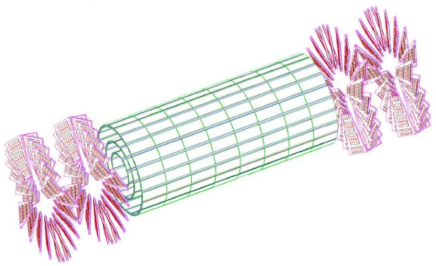

Figure 1.1: The picture shows the three barrel layers and the two disks at each end of the barrel part.

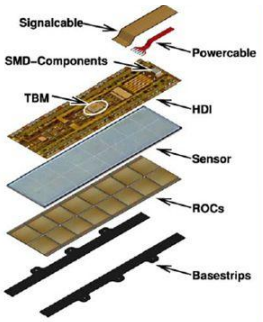

Figure 1.2: Expanded view of the Pixel Barrel Detector Module.

The pixel barrel detector module

One pixel barrel detector module comprises 16 Read Out Chips (ROCs) with 4160 channels each, where every single one is connected via indium bumps to a common pixel silicon sensor.

In figure 1.2 is shown the schematic structure of a barrel detector module. From top to bottom it is possible to see: the signal Kapton cable and the power copper cable, a High Density Interconnect (HDI), that is a low mass flexible printed circuit board (in the middle of this, a Token Bit Manager (TBM)[1] chip is positioned), silicon sensor, 16 ROC and two base strips that connect the module to the mechanical structure of the detector.

The silicon sensor has a thickness of 285μm. The pixel dimensions are 100$\times$ 150μm^2. They are realized with n-implants in a n-substrate while the backside of the sensor is p-doped (n-in-n technology). Full depletion is reached with a bias voltage of 150 V.

The ROC consists of 4160 pixels arranged in 52 columns and 80 rows. It is realized with the aim to measure the amount of charge produced in the sensor, to amplify it, to compare it to a threshold and to send it out together with the address of the hit pixel. Figure 1.3 shows how a charged particle that pass trough the depleted sensor produces holes and electrons along its track. The generated charges are then collected and brought to the ROC by the bump bonding.

1.2 LHC and CMS upgrade

In order to increase the possibilities to observe rare events that could lead to new physics and study, for example, the Higgs boson characteristics, the LHC will need a major upgrade around 2020 to increase its luminosity by a factor of 10 beyond the original design value. This necessity has given rise to the High Luminosity LHC (HL-LHC) project. This kind of upgrade must be carefully studied and also requires about 10 years to implement: new detectors must be designed and tested [2].

[1]The TBM controls the readout and programming of a module. It distributes also the first level trigger and the 40 MHz clock over the HDI to the ROCs.

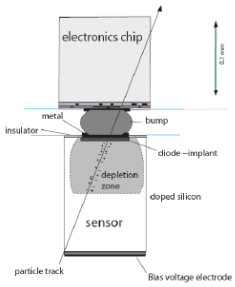

Figure 1.3: Pixel bump bonded to the ROC. This image is not in scale.

1.2.1 The CMS Phase II Tracker Upgrade

This upgrade involves the replacement of the tracker because there is the need of improved tracking performance [3]. The tracker should sustain operation with up to $200 \div 250$ collisions per bunch crossing. Thus increased granularity is required to maintain a small occupancy. The detector should provide satisfactory performance up to an integrated luminosity of about 3000 fb^{-1}, a factor of 10 more than the original design. For the innermost regions there is also the need to select more radiation hard silicon sensor material. The T-992 collaboration mission is to test silicon pixel detector prototypes for the endcaps of the pixel tracker layer of the CMS experiment for the Phase II upgrade.

Chapter 2

Test beam on pixel prototypes

The test over the pixel prototypes took place in June 2015 at Fermilab Test Beam Facility (FTBF), a high energy beam facility used for detector tests [4].

The MTest beamline has been used. It sends 120 GeV protons at a frequency between 1 and 300 kHz. The accelerator clock is set to 54 MHz and protons arrive in four second bunches every minute.

The tests over the Devices Under Testing (DUTs) were conducted using the silicon pixel and strip telescopes shown in figure 2.1.

A tracker telescope is composed by a collection of detector planes that measures the trajectory of charged particles. The DUTs were placed in the center of the telescope. Particle tracks are reconstructed using hits on the telescope planes. The pixel telescope, used during my analysis, is divided into 2 stations (one upstream and one downstream) of four planes each. The planes are silicon pixel detectors, made with PSI46 read out chips. Each ROC has 4160 pixel cells (80 rows and 52 columns). Their dimensions are $100 \times 150 \mu m^2$. In each stations there are two planes with a 2×3 grid of ROCs and two planes with a 2×4 ones. Due to the orientation of the planes, tilted at 25°, the pixel telescope has a coverage area of $\sim 2 \times 2 cm^2$. This is visible in figure 2.2. This configuration is chosen because a hit in a single pixel is readout as being located in the center of the cell, but, if a particle passes through multiple pixel cells, it may release sufficient charge to exceed a certain threshold and register a hit in each cell; so the amount of charge released in each cell can be used to accurately measure the coordinates of the hit. The 25°angle was selected in order to maximize the number of hits with 2 pixel cells.

Each station in the telescope is connected to a DAQ board, called CAPTAN, with a FPGA programmable integrated circuit that handles various processes related to data acquisition.

During the data acquisition process, pixel detectors send data to the DAQ, after receiving a trigger from a coincidence between the scintillators along the beamline. Hits are then grouped together to form an event, a set of plane hits associated with a particular trigger number.

The data acquired are first analyzed by a software package called Monicelli. Monicelli's code is written in C++ and developed by the INFN group at the University of Milano-Bicocca in Italy. It is used to precisely align the telescope and save alignments as geometry files and to reconstruct the tracks by looking at the hits on the telescope planes and then fitting a track between the points. Then another software, called Chewie, uses the output files from Monicelli to analyze the reconstructed tracks. This package was designed by the T-992 collaboration. Chewie allows to calculate the efficiency of the DUTs and creates histograms of various measurements, including efficiency, charge distribution and spatial resolution.

2.1 DUTs configuration

During my stay at Fermilab I focused my studies on one of the DUTs: DUT 0.

This detector is divided in three zones, each with pixels with a different pitch as shown in figure 2.3:

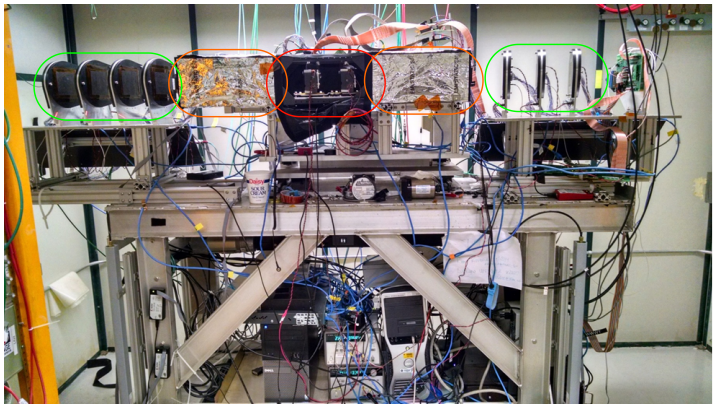

Figure 2.1: This picture shows the experimental set up. In the green circles is visible the strip telescope, in the orange ones the pixel telescope and the central red circle marks the place where the DUTs were placed.

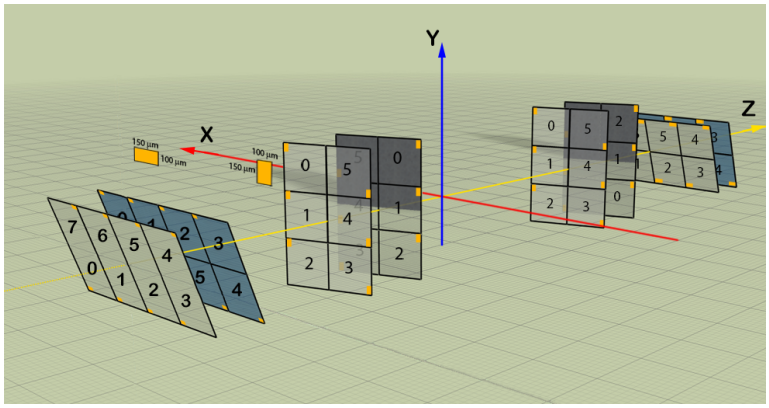

Figure 2.2: This picture shows the disposition of the various planes of the pixel telescope.

- bottom part $100 \times 150 \mu m^2$
- middle part $50 \times 300 \mu m^2$
- top part $25 \times 600 \mu m^2$

In this way all the pixels have the same area.

In in figure 2.3 are also shown the pixel's connections to the bonding. They are disposed in the same order as they are in the DUT. For the middle and the upper part are visible several rows in order to cover a dimension of $100 \mu m$. In this way is possible to see the bonding that bring the charge from the pixels to the ROC and the pattern that is repeated in each zone.

The analysis moslty focused on the $25 \times 600 \mu m^2$ pixels that have a peculiar conductive strip that passes over adjacent pixels, highlighted by the orange circles. Near the bonding, there is a capacitance of an area of $18 \mu m \times 13 \mu m$ with a SiO_2 thickness of $900 \mathring{A}$ that results on a capacitor of ~ 85 fF, to be compared with a total of ~ 200fF. This capacitor can contribute to the capacitive load for the preamplifier and the spurious charge sharing between adjacent pixel.

It is also useful to see how pixels are disposed in terms of rows and columns, figure 2.4.

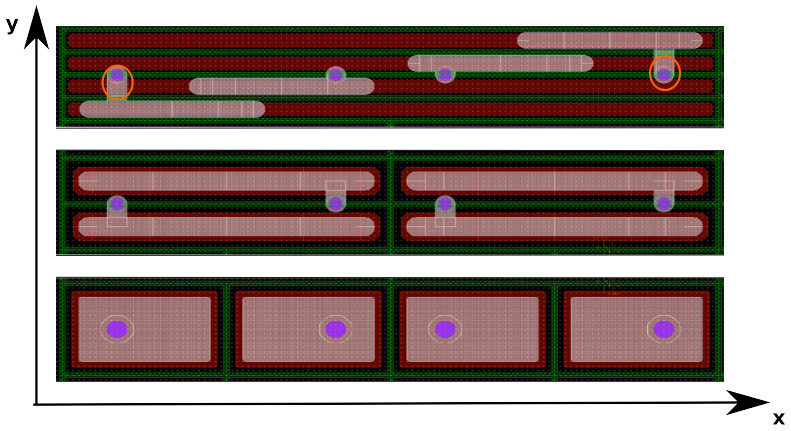

Figure 2.3: Three zones of the DUT.

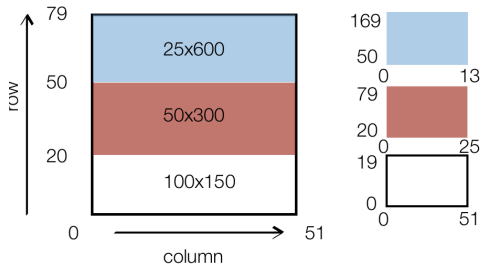

Figure 2.4: On the left the rows division for the ROC and on the right for the pixels.

Chapter 3

Data analysis

The analysis is performed separately for each zone. I used nine runs (1359, 1360, 1361, 1363, 1364, 1365, 1366, 1367, 1368, 1369). They are all biased at 120V. From now on I will refer to three different zone by the y pitch, 100μm, 50μm and 25μm.

My first task was to use Monicelli to complete the alignment of the DUTs and to reconstruct the tracks. My second task was to modify the Chewie code in order to analyze the data obtained from the three different zones of the DUTs.

I worked on the measurement of the collected charge and the spatial resolution.

I cite the efficiency results only for completeness and to prove that the three kinds of pixel are all full efficient. They are shown in figure 3.1. The efficiency mean value, computed excluding first and last rows and columns, for 100μm , 50μm and 25μm are 99.75%, 99.72% and 99.58% respectively [6].

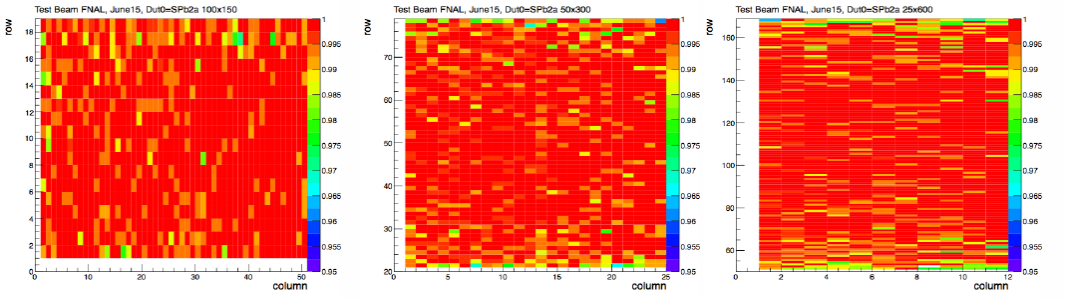

Figure 3.1: From left to right 100μm, 50μm and 25μm efficiency maps.

3.1 Charge analysis

I studied the collected charge in the three different zones in order to look at the pixel's behavior and to compare the results of the three configurations [5]. In particular I'll show some issues about the 25μm one.

In figure 3.2 is shown the collected charge in the single pixel, for each configuration. It is to be underlined that in the 25μm one there is always charge sharing between adjacent pixels because it happens in a range of $\sim$ 15μm from the hit point.

3.1.1 Clusters

A cluster is a collection of contiguous pixels with signal belonging to the same hit. As I mentioned before, the measurement of the cluster charge and of other quantities correlated to them is a help in the searching for the track impact point.

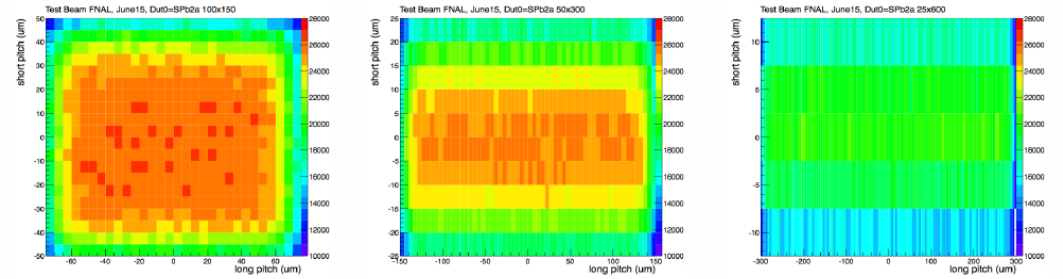

Figure 3.2: From left to right 100μm, 50μm and 25μm pixel charge maps.

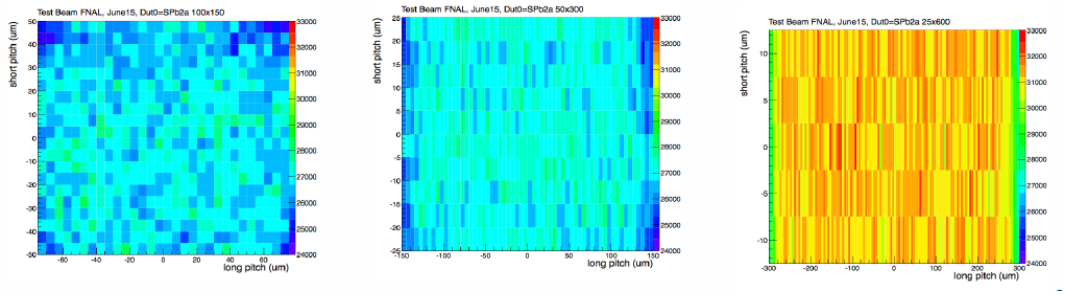

Figure 3.3: From left to right 100μm, 50μm and 25μm cluster charge maps.

One of these quantities is the cluster charge in the single pixel, figure 3.3. The 25μm configuration has a major amount of charge if compared with the others.

Cluster size

It is very important to look at the cluster size, figure 3.4. It is possible to notice that the cluster size increases as the pixel pitch decreases, but, while the 100μm and 50μm pitch pixel have clusters of size one and two, according to expectations, the 25μm has no clusters of size one but has clusters of size three and four. It is a consequence of the charge sharing and the capacitors.

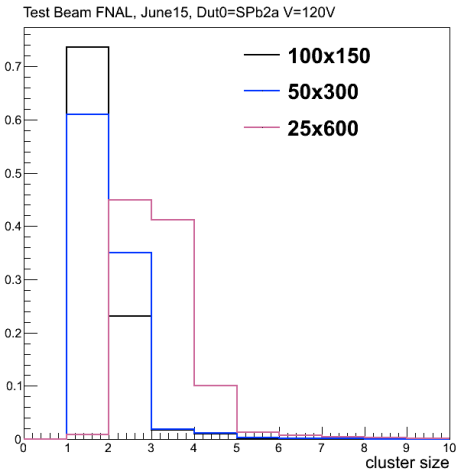

Figure 3.4: Cluster size percentage for the three different pitches. The 100μm and the 50μm behave in the same way and as expected while the 25μm has a different and unexpected behavior.

Landau distribution

I made some plots of the charge distributions. They follow a Landau distribution and are fitted with a Landau function convoluted with a Gaussian one. The Most Probable Value (MPV) is expressed in kilo electrons. It is interesting to see comparison among the different cluster sizes and the various pitch dimensions.

In figure 3.5, it is possible to notice that the distribution is a Landau with a MPV comparable with the expected one. In 3.5a there is also the ADC saturation peak.

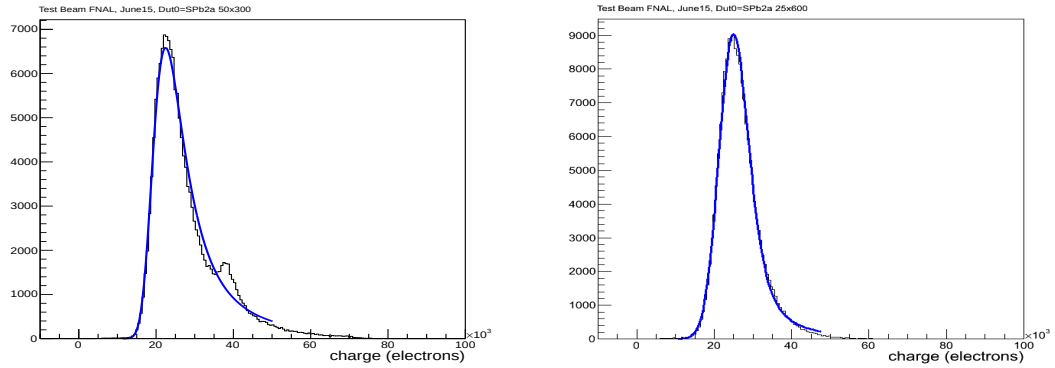

(a) 50μm, MPV $\sim$ 22 ke. (b) 25μm, MPV $\sim$ 23 ke.

Figure 3.5: Comparison between the Landau distribution of cluster of size 2 for 50μm and 25μm.

Looking at the same plots for clusters of size three, figure 3.6, we can notice a big difference in the statistics and also that in the 50μm (3.6a) the tail at high charge is caused by δ rays.

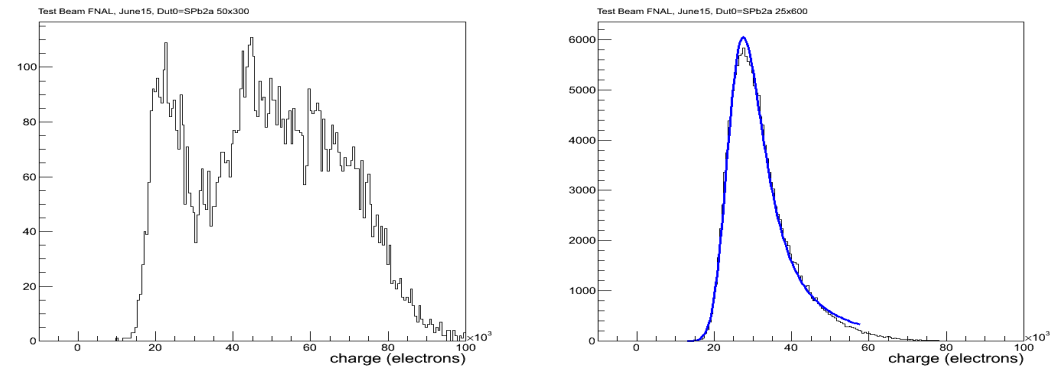

(a) 50μm, MPV $\sim$ 22 ke. (b) 25μm, MPV $\sim$ 26 ke.

Figure 3.6: Comparison between the Landau distribution of cluster of size 3 for 50μm and 25μm.

In figure 3.7b it is to be pointed out that the MPV is really high. An explanation will be given in the next pages.

3.1.2 Charge and Cluster distribution

In order to have a better understanding on what is going on in the 25μm configuration, it is important to see the results shown in figure 3.9. On the left (3.8) there is the pixels scheme, with four pixels rows (the rows will be numbered from bottom to top 1, 2, 3 e 4)with the pattern repeated in all the upper zone of the DUT. The important fact to be noticed is that all the four pixels collect the same amount of charge (3.9a) but when we look at the cluster charge (3.9b) we

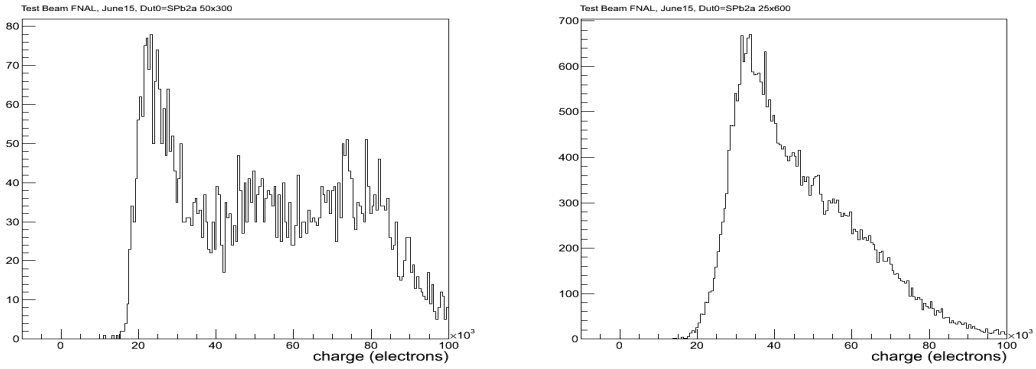

(a) 50μm, MPV $\sim$ 23 ke.

(b) 25μm, MPV $\sim$ 35 ke.

Figure 3.7: Comparison between the Landau distribution of cluster of size 4 for 50μm and 25μm.

have a major amount in the central region of the four cells configuration. This is also visible in the projection of the cluster charge along the y direction, figure 3.10.

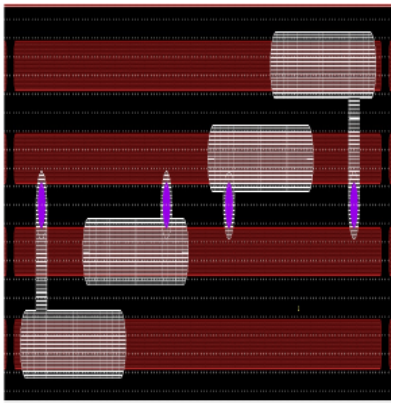

Figure 3.8: 25μm configuration, four rows.

To understand the behavior of the 25μm is useful to see what happens in the 50μm, that follows the expectations.

50μm

In this case we will look at a configuration of two rows, shown in figure 3.11.

As shown in the figure 3.12, the majority of clusters of size one happens when the track is pointing at the center of a pixel, size two when the hit is in the edge between two pixels and there is a small amount of clusters of size three. The important thing to be noticed is that all pixels behave in the same way.

25μm

I will now consider the four rows configuration (figure 3.8). In this case we see that the majority of clusters of size three happens when track is pointing in the edge between the first and the second row or the edge between the third and the for row. Cluster of size three are generated when the track is pointing in the center of the region of the 4 cells structure (rows two and three) while cluster of size four happens when the track is pointing in the edge between the second and third row.

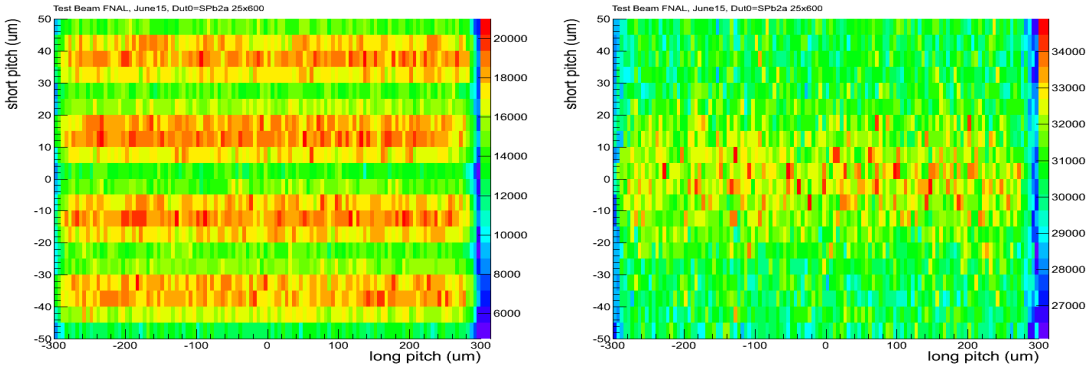

(a) 25μm configuration, four rows, pixel charge.

(b) 25μm configuration, four rows, cluster charge.

Figure 3.9: Comparison between pixel charge e cluster in a four rows configuration of 25μm.

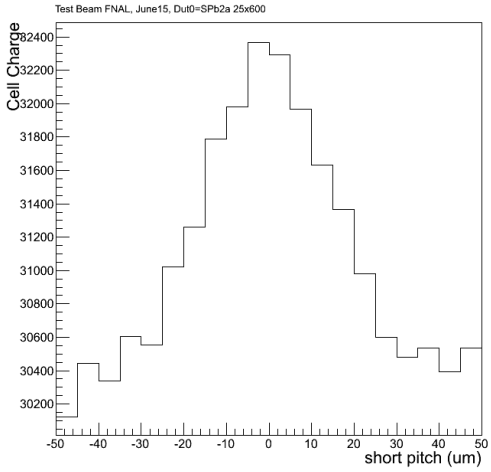

Figure 3.10: Cluster charge projected along the y direction in a four rows configuration.

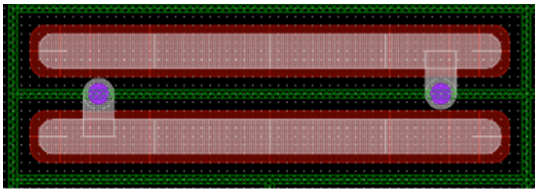

Figure 3.11: 50μm configuration, two rows.

The most important thing to notice is that the pixels of this four rows structure behave in a different ways.

The explanation of this weird behavior is due not only to the charge sharing but also to the capacitors (figure 2.3) that can induce charge among the pixels.

Charge correlation plots

In order to understand this induction among pixels I made several plots of the charge correlation in different pixels. As for the charge distribution, I'll show first what is correlation between the charge in two rows in 50μm (figure 3.14) and then in 25μm (figure 3.15, 3.16 and 3.17).

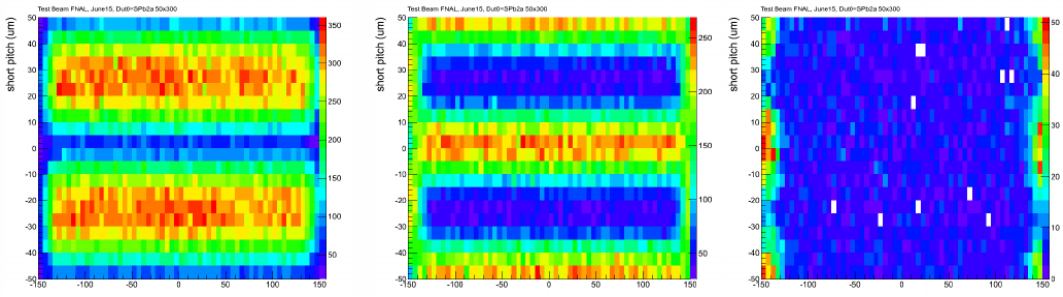

Figure 3.12: From left to right number of clusters of sizes one, two and three.

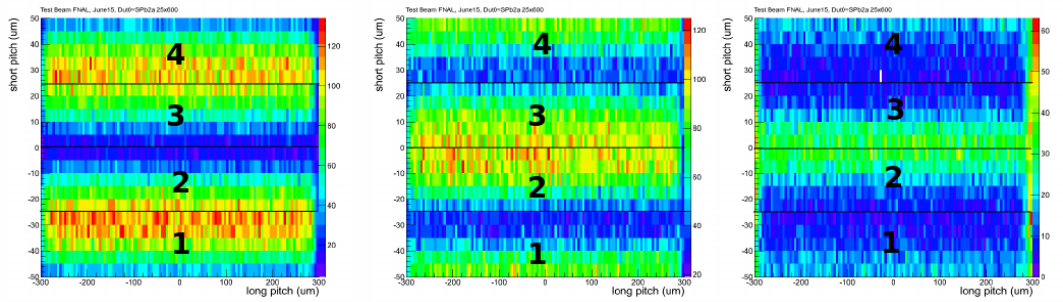

Figure 3.13: From left to right number of clusters of sizes two, three and four.

In the correlation plot for 50μm for clusters of size two (3.14a) , we can see that the two rows have the same amount of charge, and the charge value is in agreement with the Landau distribution (figure 3.5a).

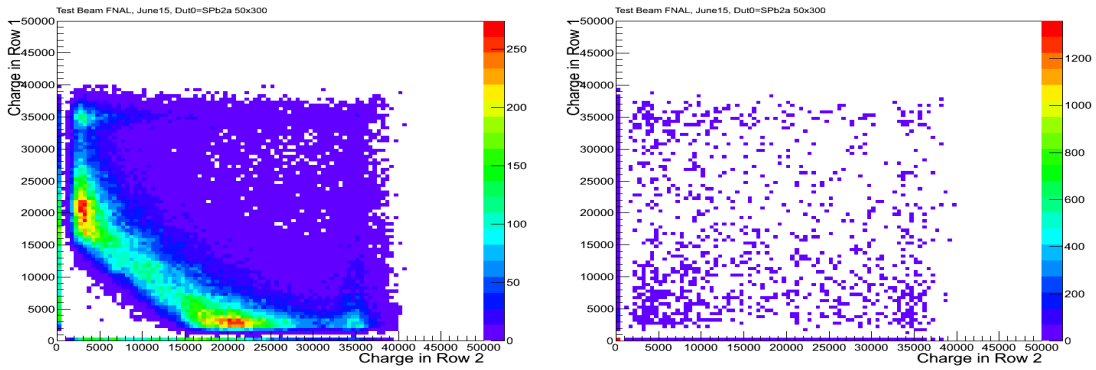

(a) 50μm, size 2.

(b) 50μm, size 4.

Figure 3.14: Comparison between pixel charge in two different rows for clusters of size two (left) and clusters of size four (right).

Looking at 3.15a, to be compared with 3.14a, we can notice a different a lack of the highest charge for row two that could have give rise to clusters of size four (3.9) and give so an explanation to the high MPV of the Landau distribution for clusters of size four (figure 3.7b).

Also, in figure 3.15b, rows 2 and 3 behave in a completely different way with respect to row 1 and 2.

Likewise, in figure 3.16, for clusters of size four, there is the same kind of correlation between rows 1 and 2 and rows 4 and 3, but is different from the one between rows 2 and 3.

In order to quantify the correlation between the different rows, I made the plots shown in figure

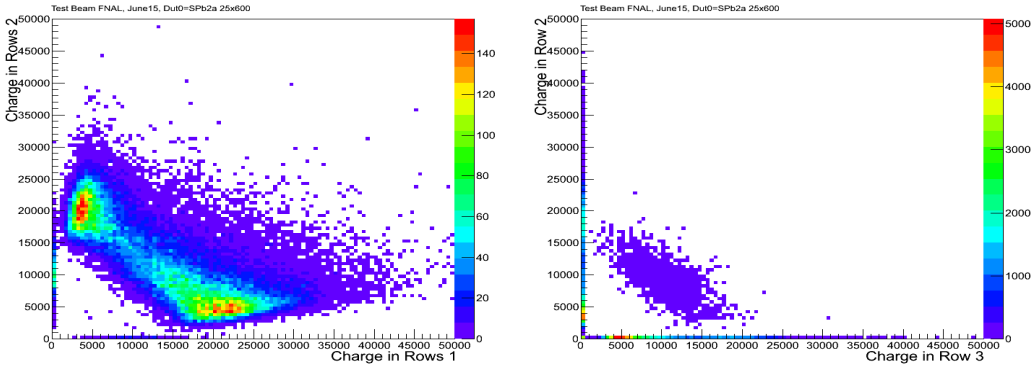

(a) 25μm, size 2, row 1 vs row 2.

(b) 25μm, size 2, row 2 vs row 3.

Figure 3.15: Comparison between the collected charge in diffinerent rows for clusters of size 2.

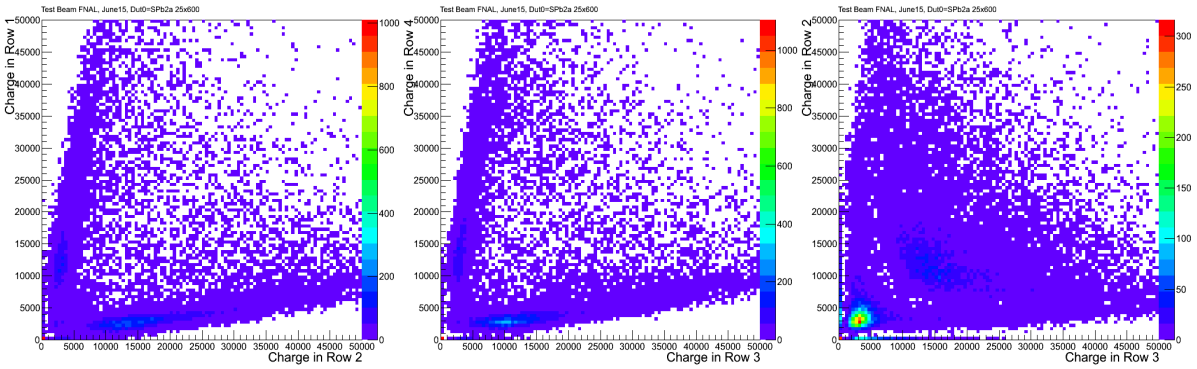

(a) 25μm, size 4, row 1 vs row 2.

(b) 25μm, size 4, row 4 vs row 3.

(c) 25μm, size 4, row 2 vs row 3.

Figure 3.16: Comparison between the collected charge in different rows for clusters of size 4.

3.17, for clusters of size four. In 3.17a on the y axis there is the sum of the charge in rows 1 and 4 and in x axis the sum of the charge in rows 2 and 3, when the track that generated the clusters is pointing on the two external rows (1 and 4). In 3.17c there is the same plots for tracks pointing in the two internal rows (2 and 3) and two axis has been exchanged to point out the similar behavior. In the second case there is more statistics, according to the right plot in 3.9.

The linear fit on the two profile (3.17b and 3.17d) lead to a slope of ~ 3 in both cases.

3.2 Spatial resolution

The analysis on the resolution has been performed using runs 1361, 1364 and 1369 that have the better alignment. Spatial resolution is calculated using the residuals.

A residual is the difference between the measured impact point and the predicted impact point from the track reconstruction.

We calculate measured impact point with two different algorithm:

- center of mass among the charges of the cluster
- asymmetry fit

The resolution is quantified using the sigma of a Gaussian fit on the residuals distribution, except some particular case that will be explained later. In both cases we applied cuts on the

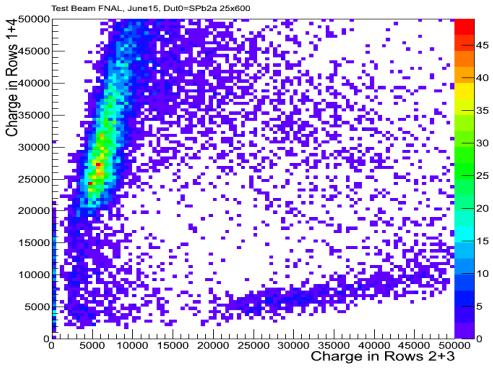

(a) 25μm, size 4, rows 1 and 4 vs rows 2 and 3, external.

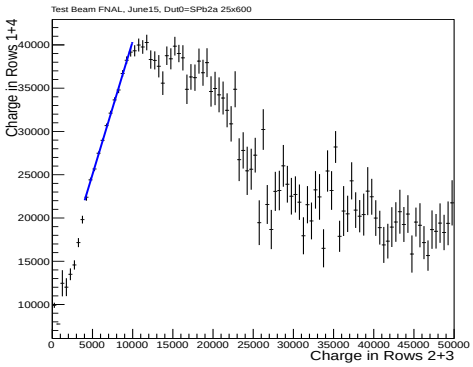

(b) 25μm, size 4, rows 1 and 4 vs rows 2 and 3, external profile.

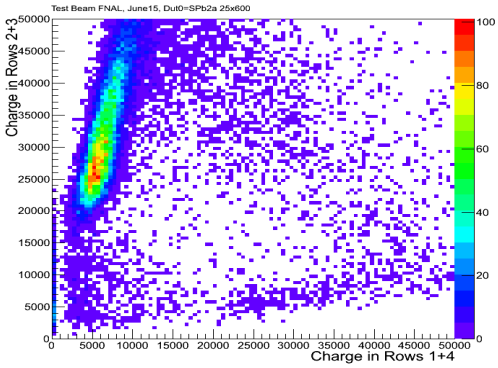

(c) 25μm, size 4, rows 2 and 3 vs rows 1 and 4, internal.

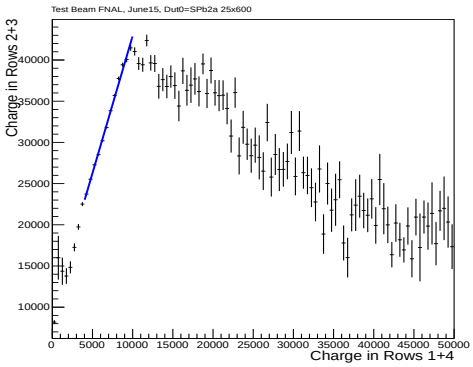

(d) 25μm, size 4, rows 2 and 3 vs rows 1 and 4, internal profile.

Figure 3.17: Correlation of the collected charge in different rows for clusters of size 4.

collected charge, selected around the Landau distribution peak for clusters of size two, and on the quality of the tracks.

The resolution that I will show contain both the contributes from the pixel telescope and the DUT.

3.2.1 Asymmetry

The asymmetry is a quantity defined for clusters of size two as the difference of the charge in the two pixels of the cluster, divided by the total cluster's charge:

$$\eta = \frac{Q_{down} - Q_{up}}{Q_{down} t Q_{up}}.$$

I used the words up and down because we are interested in clusters along the way direction.

In figure 3.18 are the asymmetry plots for the 50μm configuration. In 3.18a on the x axis there is the asymmetry and in the y axis the residual in the y direction, calculated as the difference from the predicted impact point and the measured impact point. In this case the measured impact point is the arithmetical mean between the two pixel of the cluster.

In the 3.18b there is the profile of the same plot, in order to fit it with a linear function.

We use the resulting function from the fit on the asymmetry profile to measure the impact point using the calculated asymmetry for a certain cluster of size two.

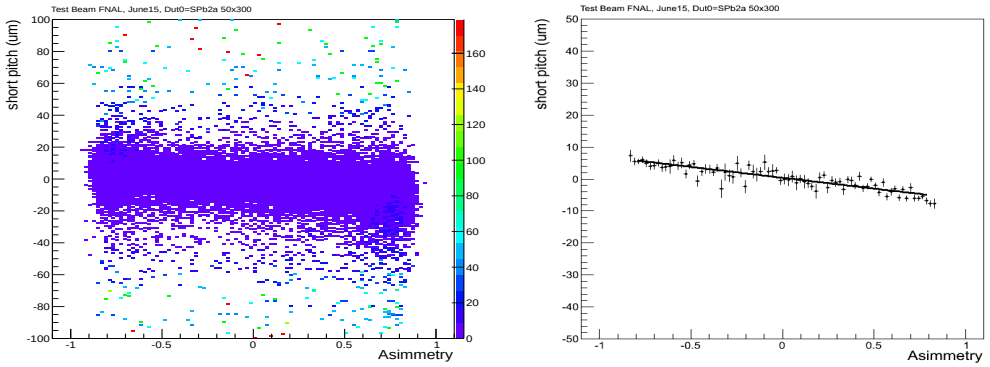

(a) 50μm, asymmetry distribution.

(b) 50μm, asymmetry linear fit.

Figure 3.18

3.2.2 Results

I'll describe the results for the three different pixel pitch size. In all the three cases the first three plots from left to right are obtained from the center of mass method for different clusters size while the one on the right is obtained using the asymmetry fit.

I'll start to describe the results from the standard pitch configuration (100μm), shown in figure 3.19.

It is to be pointed out that in this case, for clusters of size one it was not used a Gaussian fit because we have a superposition of a Gaussian and a flat distribution. This is due to the fact that in the center of this kind of pixel there is no charge sharing so in central region each point has the same probability to be hit by the track and this lead to the flat distribution. In this case the measured resolution is 25.8μm, resulting from the width of the fit divided by the square root of 12[1]

For clusters of size two we used a Gaussian fit and the measured resolution is 11μm.

For all clusters the we didn't use a Gaussian fit, due to the contribute from clusters of size one. In this case the resolution is measured from the RMS of the distribution restricted to the range $\pm$50μm and is 24μm.

For clusters of size two, the resolution coming from the center of mass algorithm has to be compared with the ones coming from the asymmetry fit, 7.5μm.

Looking at the 50μm configuration, figure 3.20, from the center of mass method we measure a resolution of 12.68μm for all clusters size, 12.96μm for clusters of size one and 11.25μm for clusters of size two while from asymmetry we have 7.8μm.

Finally, looking at the 25μm configuration, figure 3.21, from the center of mass method we measure a resolution of 9.9μm for all clusters size, the population is negligible for clusters of size one and 8.7μm for clusters of size two while from asymmetry we have 7.4μm.

In this last case is important to point out that the center of the distribution is in -1.04μm because if we look at the same distribution for the four different rows, figure 3.22, the sigma of the distribution is always around 6.5μm but the mean value is, from left to right 1.9μm, -5.9μm, 2.8μm and -4.3μm.

This point out that the Gaussian distribution for the residuals of size two in the 25μm configuration, calculated from the asymmetry fit, is the sum of these four Gaussian distribution. The fact that they are not centered in zero could be a consequence of different behavior of the pixel 1(4) and 2(3).

[1]The variance of the uniform distribution is

$$\sigma^2 = \frac{(b-a)^2}{12}$$

where a and b are the extremes of the distribution. In stead of their difference we use the width resulting from the fit.

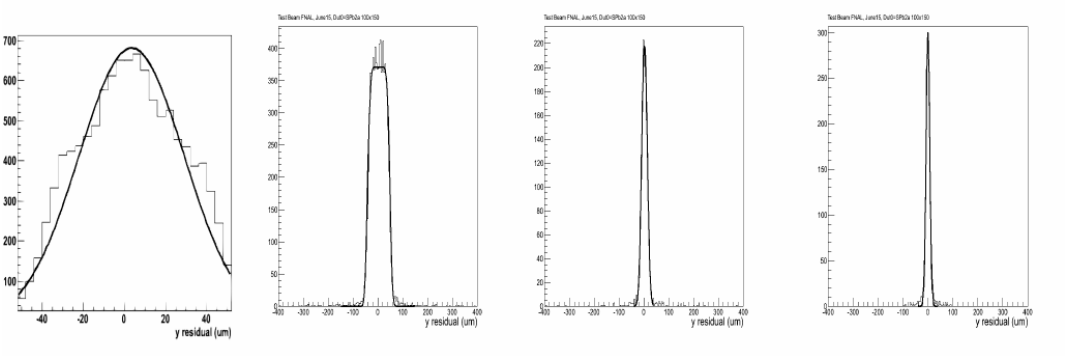

Figure 3.19: 100μm: from left to right, resolution measured using the center of mass method for all size cluster, clusters of size one, clusters of size two and resolution measured using the asymmetry fit for clusters of size two.

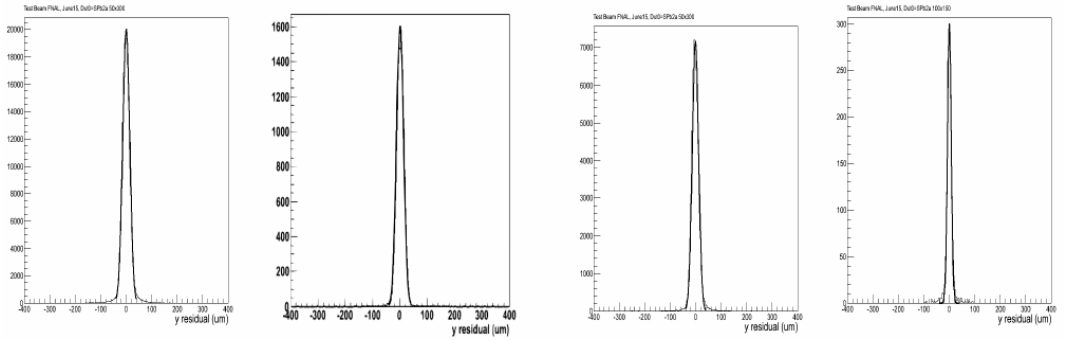

Figure 3.20: 50μm: from left to right, resolution measured using the center of mass method for all size cluster, clusters of size one, clusters of size two and resolution measured using the asymmetry fit for clusters of size two.

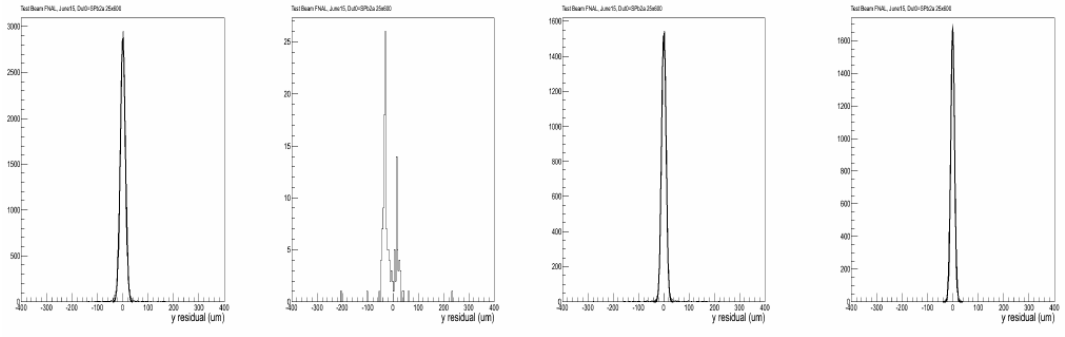

Figure 3.21: 25μm: from left to right, resolution measured using the center of mass method for all size cluster, clusters of size one, clusters of size two and resolution measured using the asymmetry fit for clusters of size two.

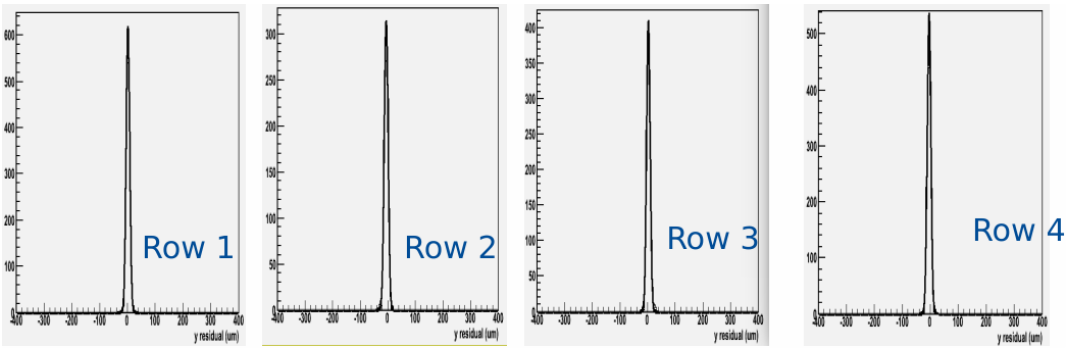

Figure 3.22: 25μm: from left to right, row 1, 2, 3 and 4.

Conclusions

It is possible to state that the devices are fully efficient independently of the pitch.

The cluster size varies with the pitch as expected, except for 25μm. For this configuration we have an unexpected amount of clusters of size four.

There is still work to do on the understanding of the impact of the extra capacitance, but looking at the results coming from the collected charge, we can conclude that the capacitors induce charge among the pixels. In particular we think that they are responsible for the clusters of size four: when the track is pointing in the edge between row 2 and row 3 there is not only charge sharing between these two pixels but induction on the pixels of row 1 and 4 due to this conductive strip. We are trying to make corrections for these effects.

The spatial resolution, for clusters of size two, with the use of the asymmetry fit, is comparable in all the three zones as expected.

Bibliography

[1] Sarah Dambach, *CMS Pixel Module Readout Optimization and Study of the B0 Lifetime in the Semileptonic Decay Mode.*

[2] http://hilumilhc.web.cern.ch/

[3] A. Tricomi, *Upgrade of the CMS tracker*, Jinst 9 C03041, 2014.

[4] David Gonzalez-Dysinger, *Synchronization of the Pixel and Strip Telescopes at the Fermilab Test Beam Facility.*

[5] Ivette Bermudez, *Small pitch pixel detector for the CMS phase II upgrade.*

[6] Caterina Vernieri, *CMS Physics & Upgrade Week Ischia, 09.8.15, Pixel-Phase-II R&D at FNAL.*